REPORT

OF

PORT AND HARBOUR TECHNICAL RESEARCH INSTITUTE

REPORT No. 9

The Generation of Water Waves with a Vertically Oscillating Flow at a Channel Bottom

by

Yoshimi Goda

Tooru Kikuya

August 1964

PORT AND HARBOUR TECHNICAL RESEARCH INSTITUTE
MINISTRY OF TRANSPORTATION

162 Kawama, Yokosuka-City, Kanagawa-Prefecture, Japan

運輸技術政策総合研究所
図書室
蔵書

THE GENERATION OF WATER WAVES WITH A VERTICALLY OSCILLATING FLOW AT A CHANNEL BOTTOM

By Yoshimi GODA* and Tooru KIKUYA**

CONTENTS

LIST OF TABLES AND FIGURES

* Chief of Model Test Section, Hydraulics Division, Sc. M.
** Breakwater Laboratory, Hydraulics Division.

SYNOPSIS

A regular train of water waves can be generated with a vertically oscillating flow at a channel bottom. The solution of velocity potential for such flow-generated waves has been obtained, and expressions for wave profiles and bottom pressure are presented. Results of a small scale test for this type of wave generator show fair agreement with the theory developed: the generated wave heights being 80 per cent of analytical ones and the force required to drive an underwater piston being some 20 per cent larger than analytical ones. The reflection coefficient of the wave generator was also found to be 16 per cent in terms of wave height.

Because of this low reflection coefficient, this type of wave generator is a very promising one to be fitted to an experimental wave tank which has been troubled with the problems of multi-wave-reflection between the wave paddle and model structures under study.

"鉛直振動流による造波方式について"

合田良実, 菊谷　徹

要　旨

通常の造波装置では，模型で反射された波が再び造波部分で反射されて実験に使う波を歪める欠点がある。本報告で取り上げたのは，水路の底から出入する鉛直振動流によって波を発生させる造波方式で，造波部からの反射率は実験の結果約16%と推定され，造波部からの反射波が極めて小さい特徴がある。

この方式によって生ずる波については，その速度ポテンシャルがフーリエ変換を利用して求められ，発生波高および造波部の圧力の計算式が導かれた。実験結果では，発生波高が理論値の80%，造波ピストンに作用する力が計算値の120%となった。

LIST OF SYMBOLS*

A_0 = amplitude of original progressive wave
b = half-width of wave generating slot
B = width of channel
e = amplitude of piston movement
$f(x, z)$ = function for velocity potential (see Eq. 4)
$F(u, z)$ = Fourier transformation of $f(x, z)$ (see Eq. 7)
F = force required to drive the piston
g = acceleration of gravity
$g(w)$ = integrand function for $G(\xi, z)$ (see Eq. 19)
$G(\xi, z)$ = nominal function for $f(x, z)$ (see Eqs. 17 and 18)
h = water depth
H = generated wave height
H_s = standing wave height
H_o = height of original progressive wave
i = imaginary number ($=\sqrt{-1}$)
k = wave number of $2\pi/L$ (see Eq. 24)
k_n = imaginary wave number (see Eq. 25)
K_R = reflection coefficient in terms of wave height
l = distance between a vertical wall and the source of partial reflection
L = wave length
n = integer ($=1, 2, 3, \ldots\ldots$)
p = bottom pressure
P = total pressure over the wave generating area
$R(\alpha)$ = residue of $g(w)$ at pole of $w=\alpha$
t = time
T = wave period
u = integration variable for $f(x, z)$
U = maximum velocity of vertically oscillating flow
w = complex variable for the integration of $g(w)$
W = weight of water mass moving in the same phase with the piston
$\overline{\dot{W}}$ = average rate of work done by oscillating flow
x = horizontal coordinate measured from the center of wave generation
z = vertical coordinate measured upward from the channel bottom
$_i$ = subscript referring to the inside of wave generating area
$_o$ = subscript referring to the outside of wave generating area

* Only the most commonly used notations are defined here. Notations not generally used throughout the study are defined only in their place of usage.

$_s$ =subscript referring to standing wave

α =pole of $g(w)$

ζ =retrogressive wave profile

η =progressive wave profile

ξ =parameter standing for $x+b$ or $x-b$ (see Eq. 18)

π =constant (3.14159.....)

ρ =density of water

σ =angular frequency of $2\pi/T$

ϕ =velocity potential

$\emptyset$ =solution of velocity potential for flow generated waves.

I. INTRODUCTION

In the planning and design of harbor structures and coast protection works, model experiments are indispensable tools for engineers. The stability of a proposed breakwater against wave actions, the crown height of a sea wall to prevent the overtopping of waves, and the most effective arrangement of breakwaters to shelter a harbor from waves, are a few examples of the problems which can be solved successfully through some scale tests. These model tests and other fundamental experiments are carried out in a test flume or tank which is provided with some wave maker.

One of the problems inherent to model tests is the simulation of the open sea where all outgoing waves die away in its vast area. The model test has to be carried out in the bounded area of a wave tank. Waves propagating toward a vertical wall of the wave tank are reflected at the wall and tend to disturb the original wave system, unless some devices of wave energy dissipation are provided. For this purpose wave absorbers are installed at the end of a wave tank and, in some cases, along the side walls too. But in the case of the stability test of a vertical-wall breakwater, incident waves may be reflected totally by the model breakwater. If the wave maker is made of a vertical plate moving back and forth, or up and down, the waves reflected by the model breakwater will be reflected again by the wave maker and disturb the incident waves to the breakwater; hence the test can not be continued any more.

The current technique to avoid this multi-reflection of test waves is either to complete the test before the arrival of reflected waves or to install wave filters in front of the wave maker. But neither method is satisfactory; the fromer for its short time available and the latter for still remaining reflected waves.

A promising method to solve this multi-reflection problem is to generate the waves with a vertically oscillating flow at the bottom of a wave channel. This can be done with an underwater piston which moves up and down in a vertical cylinder connected to the channel bottom. Since this type of wave maker does not have a vertical plate which causes the wave reflection, it is considered that there will be little reflection from the wave maker. Actually a similar type of wave maker has been constructed at Kyoto University in 1960 and has been used for the study of wave overtoppings for sea walls (Iwagaki et. al. 1962). But it seems to the authors that there has been no analysis of the wave generation mechanism and little information is available for the efficiency of wave generation and the power required for it.

Hence an attempt has been made to develop a theory of the wave generation for this type of wave maker so that engineers can design the wave maker with some confidence and proceed in their model studies in the field of coastal engineering. The present report deals with the development of the theory and discusses the comparison of theoretical wave generating efficieny with some experimental data.

II. THEORY OF WAVE GENERATION WITH A VERTICALLY OSCILLATING FLOW

Foundamental Equation and Boundary Conditions

Let us presume the existence of the velocity potential, ϕ, which satisfies the Laplace's equation:

$$\frac{\partial^2\phi}{\partial x^2}+\frac{\partial^2\phi}{\partial z^2}=0 \quad \cdots\cdots(1)$$

The boundary conditions are given at the water surface, $z=h$, and along the channel bottom, $z=0$. With the assumptions of small amplitude motion and of uniformly oscillating vertical flow of $U\cos\sigma t$ at the slot of the channel bottom from $x=-b$ to $x=b$, the boundary conditions are expressed as (see Fig. 1):

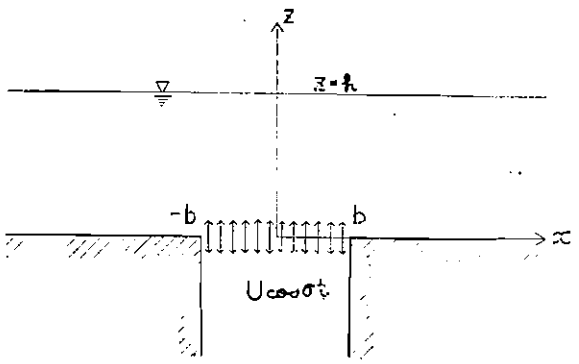

Fig. 1. Definition Sketch of Coordinate System

$$\frac{\partial\phi}{\partial z}=\begin{cases}-U\cos\sigma t & \text{for } |x|\leq b \text{ at } z=0\\ 0 & \text{for } |x|>b \text{ at } z=0\end{cases} \quad \cdots\cdots(2)$$

$$\frac{\partial^2\phi}{\partial t^2}+g\frac{\partial\phi}{\partial z}=0 \quad \text{at } z=h \quad \cdots\cdots(3)$$

in which U denotes the magnitude of oscillating flow, σ is the angular frequency of $2\pi/T$ with the wave period being T, and t is time. We may also add one more condition to the above ones; that is, the velocity potential shall have the form of progressive waves at $x=\pm\infty$ after Stoker 1960 (p. 59).

Since we are seeking the solution for the velocity potential of oscillating form in two dimensional domain, the velocity potential can be written in the following form:

$$\phi(x, z; t) = -f(x, z)\cos\sigma t \quad \cdots\cdots(4)$$

Then the function $f(x, z)$ must satisfy the Laplace's equation and the boundary conditions of

$$\left(\frac{\partial f}{\partial z}\right)_{z=0} = \begin{cases} U & \text{for } |x| \le b \\ 0 & |x| > b \end{cases} \quad \cdots\cdots(5)$$

$$\left(\frac{\partial f}{\partial z}\right)_{z=h} - \frac{\sigma^2}{g} f(x, h) = 0 \quad \cdots\cdots(6)$$

Fourier Transformation of $f(x, z)$

The solution for $f(x, z)$ can be obtained by means of the Fourier transformation. Let $F(u, z)$ be the Fourier transform of $f(x, z)$ such that,

$$F(u, z) = \int_{-\infty}^{\infty} e^{-ius} f(s, z)\, ds \quad \cdots\cdots(7)$$

$$f(x, z) = \frac{1}{2\pi}\int_{-\infty}^{\infty} e^{iux} F(u, z)\, du \quad \cdots\cdots(8)$$

The Laplace's equation and boundary conditions for $f(x, z)$ are then rewritten for $F(u, z)$ as

$$-u^2 F(u, z) + \frac{\partial^2 F}{\partial z^2} = 0 \quad \cdots\cdots(9)$$

$$\left(\frac{\partial F}{\partial z}\right)_{z=0} = \frac{2U\sin ub}{u} \quad \cdots\cdots(10)$$

$$\left(\frac{\partial F}{\partial z}\right)_{z=h} = \frac{\sigma^2}{g} F(u, h) \quad \cdots\cdots(11)$$

Since the general solution of Eq. 9 is given by

$$F(u, z) = C_1(u) e^{uz} + C_2(u) e^{-uz} \quad \cdots\cdots(12)$$

the simultaneous equations for $C_1(u)$ and $C_2(u)$ are obtained from Eqs. 10 and 11 as:

$$C_1(u) - C_2(u) = \frac{2U\sin ub}{u^2} \quad \cdots\cdots(13)$$

$$\left(u - \frac{\sigma^2}{g}\right) e^{uh} C_1(u) - \left(u + \frac{\sigma^2}{g}\right) e^{-uh} C_2(u) = 0 \quad \cdots\cdots(14)$$

By determining the parametric constants $C_1(u)$ and $C_2(u)$ from Eqs. 13 and 14, the function $F(u, z)$ is obtained as:

$$F(u, z) = \frac{U\sin ub[(ug+\sigma^2) e^{u(z-h)} + (ug-\sigma^2) e^{-u(z-h)}]}{u^2(\sigma^2 \cosh uh - ug \sinh uh)} \quad \cdots\cdots(15)$$

Evaluation of $f(x, z)$ through a Complex Integration

With the transformation function $F(u, z)$ being determined in Eq. 15, the function $f(x, z)$ is recovered with the relation of Eq. 8 as:

$$f(x,z)=\frac{U}{\pi}\int_{-\infty}^{\infty}\frac{e^{iux}\sin ub[ug\cosh u(z-h)+\sigma^2\sinh u(z-h)]}{u^2[\sigma^2\cosh uh-ug\sinh uh]}du$$

$$=\frac{U}{2\pi i}\int_{-\infty}^{\infty}\frac{ug\cosh u(z-h)+\sigma^2\sinh u(z-h)}{u^2[\sigma^2\cosh uh-ug\sinh uh]}[e^{iu(x+b)}-e^{iu(x-b)}]\,du \quad \cdots\cdots(16)$$

If we introduce the following function $G(\xi, z)$

$$G(\xi,z)=\int_{-\infty}^{\infty}\frac{e^{iu\xi}[ug\cosh u(z-h)+\sigma^2\sinh u(z-h)]}{u^2(\sigma^2\cosh uh-ug\sinh uh)}du \quad \cdots\cdots(17)$$

then the function $f(x, z)$ is expressed with $G(\xi, z)$ as:

$$f(x,z)=\frac{U}{2\pi i}[G(x+b,z)-G(x-b,z)] \quad \cdots\cdots(18)$$

Thus the problem is to evaluate the integration in Eq. 17 so as to obtain an explicit form of $f(x, z)$.

The integration can be evaluated by the method of complex integration. Let us consider the following integration with the complex variable, w, in the $u-v$ plane:

$$I_w=\int_C g(w)\,dw \quad \cdots\cdots(19)$$

in which $g(w)$ is the integrand of Eq. 17 with the integration variable, u, being replaced by the complex variable, w. The contour of the integration is taken as a semi-circle with detours at $w=-k$, 0, and k in the upper half of $u-v$ plane for $\xi>0$ and in the lower half for $\xi\leq 0$, as sketched in Fig. 2. The detours are so provided to avoid the poles on the u-axis.

Applying the Cauchy's residue theorem, the integration of Eq. 17 is rewritten as:

$$I_w=\int_{S_A}g(w)\,dw+\int_{-A}^{-k-r}g(w)\,dw+\int_{S_{-k}}g(w)\,dw+\int_{-k+r}^{-r}g(w)\,dw$$

$$+\int_{S_0}g(w)\,dw+\int_{r}^{k-r}g(w)\,dw+\int_{S_k}g(w)\,dw+\int_{k+r}^{A}g(w)\,dw$$

$$=\pm 2\pi i\sum_{n=1}^{m}R(\alpha_n) \quad \cdots\cdots(20)$$

in which S_A denotes a semi-circle from A through $-A$, S_{-k}, S_0 and S_k for the detours at $w=-k$, 0 and k with a radius of r, $R(\alpha_n)$ is the residue of the pole at $w=\alpha_n$, and m is the number of poles. The upper sign of the double signs in the right hand side of Eq. 20 is for $\xi>0$ and the lower sign for $\xi\leq 0$; this notation for the double signs is applied throughout this section.

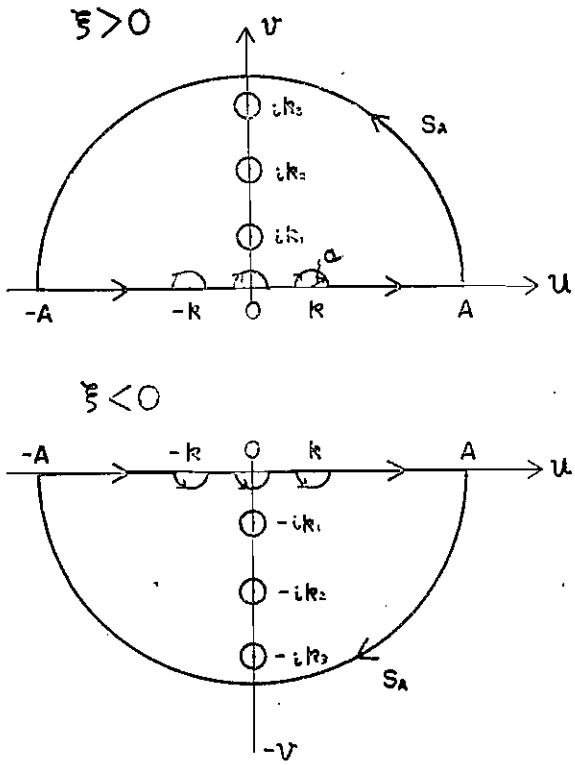

Fig. 2. Integration Contours

As it can be seen readily, the part of the complex integration along the u-axis from $-A$ to A is the same with the integration in Eq. 17, provided the radius A being extended to infinity and the radius r being reduced to zero. Therefore $G(\xi, z)$ can be obtained from the following equation:

$$G(\xi, z)=\lim_{\substack{r\to 0\\ A\to\infty}}\left\{\pm 2\pi i\sum_{n=1}^{m}R(\alpha_n)-\int_{S_A}g(w)\,dw-\int_{S_{-k}}g(w)\,dw\right.$$
$$\left.-\int_{S_0}g(w)\,dw-\int_{S_k}g(w)\,dw\right\} \quad \cdots\cdots(21)$$

The terms in the right hand side of the above equation are evaluated one by one as shown in the following.

First, the singular points of $g(w)$ are obtained as the zero points of the denominator, i. e.,

$$w=0 \quad \cdots\cdots(22)$$
$$\sigma^2=gw\tanh wh \quad \cdots\cdots(23)$$

Equation 23 has the solution of $w=-k$ and k, and $w=-ik_n$ and ik_n such that

$$\sigma^2=gk\tanh kh \quad \cdots\cdots(24)$$
$$\sigma^2=-gk_n\tan k_nh \quad \cdots\cdots(25)$$

These equations determine the locations of the poles of $g(w)$. The condition of

Eq. 24 is just the same as that describing the wave number of $2\pi/L$ for the small amplitude water waves with the wave length of L. Actually k is shown to be the wave number as seen in later sections.

Second, the integration along the large circle S_A from A to $-A$ is shown to go to zero as A is extended to infinity. Since the functions, $\tanh wh$ and $\tanh w(z-h)$, approach unity as w increases, the limit of the integration with $A\to\infty$ is expressed as:

$$\lim_{A\to\infty}\left|\int_{S_A} g(w)\,dw\right| = \lim_{A\to\infty}\left|\int_{S_A} \frac{e^{iw\xi}\cosh w(z-h)[1+\sigma^2\tanh w(z-h)/wg]}{w^2\sinh wh[\sigma^2/(wg\tanh wh)-1]}\,dw\right|$$
$$\leq \lim_{A\to\infty}\left|\int_{S_A} \frac{e^{iw\xi}\cosh w(z-h)}{w^2\sinh wh}\,dw\right|$$
$$\leq \lim_{A\to\infty}\left|\int_{S_A} \frac{e^{iw\xi}}{w^2}\,dw\right|$$

Since the contour of the integration is taken at the upper domain of w for $\xi>0$ and at the lower domain of w for $\xi\leq 0$, the numerator of the above integrand does not exceed unity. Hence,

$$\lim_{A\to\infty}\left|\int_{S_A} g(w)\,dw\right| \leq \lim_{A\to\infty}\left|\pm\int_0^{\pi}\frac{A\,d\theta}{A^2e^{2i\theta}}\right| \leq \lim_{A\to\infty}\frac{\pi}{A}=0 \qquad \cdots\cdots(26)$$

Third, three integrations along detours at $w=-k$, 0, and k are evaluated with the residues $R(-k)$, $R(0)$, and $R(k)$ as:

$$\lim_{r\to 0}\left\{\int_{S_{-k}} g(w)\,dw+\int_{S_0} g(w)\,dw+\int_{S_k} g(w)\,dw\right\} = \mp\pi i[R(-k)+R(0)+R(k)] \qquad \cdots\cdots(27)$$

These residues are calculated as:

$$\begin{cases} R(k)=\left[\dfrac{N(w)}{D'(w)}\right]_{w=k}=-\dfrac{2e^{ik\xi}\cosh kz}{k(\sinh 2kh+2kh)} \\ R(-k)=\left[\dfrac{N(w)}{D'(w)}\right]_{w=-k}=-\dfrac{2e^{-ik\xi}\cosh kz}{k(\sinh 2kh+2kh)} \\ R(0)=\left[\dfrac{N(w)}{D'(w)}\right]_{w=0}=(z-h)+\dfrac{1}{k\tanh kh} \end{cases} \qquad \cdots\cdots(28)$$

in which $N(w)$ stands for the numerator of $g(w)$ and $D'(w)$ is the derivative of the denominator of $g(w)$. Hence,

$$\lim_{r\to 0}\left\{\int_{S_{-k}} g(w)\,dw+\int_{S_0} g(w)\,dw+\int_{S_k} g(w)\,dw\right\}$$
$$=\pm\pi i\left[\frac{4\cosh kz\cos k\xi}{k(\sinh 2kh+2kh)}-\frac{1}{k\tanh kh}+(h-z)\right] \qquad \cdots\cdots(29)$$

Fourth, the residues at singular points at $w=ik_n$ and $-ik_n$ are evaluated in the same way as those in Eq. 28. The results are written as:

$$R(\pm ik_n)=2\frac{e^{\mp k_n\xi}\cos k_nz}{k_n(\sin 2k_nh+2k_nh)} \quad \cdots\cdots(30)$$

Substituting the results of the calculations, Eqs. 26, 29, and 30, into Eq. 21, we obtain the function $G(\xi, z)$ in the following form:

$$G(\xi, z)=\pm\pi i\left\{4\sum_{n=1}^{\infty}\frac{e^{\mp k_n\xi}\cos k_nz}{k_n(\sin 2k_nh+2k_nh)}-4\frac{\cosh kz\cos k\xi}{k(\sinh 2kh+2kh)}\right.$$
$$\left.+\frac{1}{k\tanh kh}+(z-h)\right\} \quad \cdots\cdots(31)$$

As stated before, the upper signs of the double signs in the right hand side of the above equation are for $\xi>0$ and the lower signs for $\xi\leq 0$,

The function $f(x, z)$ is now calculated from Eq. 18 with $G(\xi, z)$ obtained in Eq. 31. The calculation must be done separately for three ranges of x: i. e., $x>b$, $b>x>-b$, and $-b>x$.

For the first range of $x>b$,

$$f_o(x, z)=4U\left\{\frac{\cosh kz\sin kx\sin kb}{k(\sinh 2kh+2kh)}-\sum_{n=1}^{\infty}\frac{e^{-k_nx}\sinh k_nb\cos k_nh}{k_n(\sin 2k_nh+2k_nh)}\right\} \quad \cdots\cdots(32)$$

For $b>x>-b$,

$$f_i(x, z)=4U\left\{4\sum_{n=1}^{\infty}\frac{e^{-k_nb}\cosh k_nx\cos k_nz}{k_n(\sin 2k_nh+2k_nh)}-4\frac{\cos kb\cos kx\cosh kz}{k(\sinh 2kh+2kh)}\right.$$
$$\left.+(z-h)+\frac{1}{k\tanh kh}\right\} \quad \cdots\cdots(33)$$

For $-b>x$,

$$f_o(x, z)=-4U\left\{\frac{\sin kb\sin kx\cosh kz}{k(\sinh 2kh+2kh)}+\sum_{n=1}^{\infty}\frac{e^{k_nx}\sinh k_nb\cos k_nz}{k_n(\sin 2k_nh+2k_nh)}\right\} \quad \cdots\cdots(34)$$

It is shown that the above solutions of $f(x, z)$ satisfy the Laplace's equation and the boundary conditions of Eqs. 5. and 6.

With the function $f(x, z)$ evaluated in the above, the velocity potential is described in Eq. 4.

The Solution of Generated Wave Profile

Since the Laplace's equation and the boundary conditions are linear with respect to ϕ, we may superimpose a velocity potential of the following form, ϕ_s, in order to obtain the velocity potential for progressive waves:

$$\phi_s=f_s(x, z)\sin\sigma t \quad \cdots\cdots(35)$$

where:

$$f_s(x, z)=4U\frac{\sin kb\cos kx\cosh kz}{k(\sinh 2kh+2kh)} \quad \cdots\cdots(36)$$

The new velocity potential thus formed is written for the range of $|x|>b$ as:

$$\Phi_o=\phi_o+\phi_s=-f_o(x,\ z)\cos\sigma t+f_s(x,\ z)\sin\sigma t$$

$$=-4U\left\{\frac{\sin kb\cosh kz}{k(\sinh 2kh+2kh)}\sin(k|x|-\sigma t)\right.$$

$$\left.+\sum_{n=1}^{\infty}\frac{e^{-k_n|x|}\sinh k_nb\cos k_nz}{k_n(\sin 2k_nh+2k_nh)}\cos\sigma t\right\} \quad \cdots\cdots(37)$$

The expression for the new velocity potential for the range of $|x|<b$ is presented in the next section for the pressure variation, because the profiles of generated waves away from the generating area are of major interest at present.

The water surface profile is then obtained from this velocity potential as:

$$\eta=\frac{1}{g}\left[\frac{\partial\Phi_o}{\partial t}\right]_{z=h}$$

$$=\frac{4U}{\sigma}\left\{\frac{\sinh kh\sin kb}{\sinh 2kh+2kh}\cos(k|x|-\sigma t)+\sum_{n=1}^{\infty}\frac{e^{-k_n|x|}\sinh k_nb\sin k_nh}{(\sin 2k_nh+2k_nh)}\sin\sigma t\right\}$$

$$\cdots\cdots(38)$$

The first term of Eq. 38 clearly indicates that two trains of waves with the same amplitude are generated and propagate away from the generating area toward $x=\infty$ and $x=-\infty$. The second term which is in actual an infinite series represents a distrubance centered around the generating area. The disturbance diminishes its magnitude rapidly as it goes far from the generating area. In most cases the magnitude of this disturbance will be neglected in comparison with that of the first term. Table 1 shows the result of a numerical evaluation of the first and second term for the condition of $kh=kb=1$. This example clearly illustrates the rapid decrease of the second term with the increase of x.

TABLE 1. Magnitude of Disturbance in Terms of Wave Amplitude for $kh=kb=1$.

x/b	Second Term/First Term				
	$n=1$	$n=2$	$n=3$	remainder	sum
1.00	0.114	0.024	0.010	0.026	0.174
1.25	0.055	0.005	0.001	—	0.061
1.50	0.027	0.001	—	—	0.028
1.75	0.013	—	—	—	0.013
2.00	0.006	—	—	—	0.006

If the oscillating flow is produced with a horizontal plate moving vertically in sinusoidal manner with an amplitude of e and the angular frequency of σ, the velocity U is replaced with $e\sigma$. The wave profile away from the generating area is then expressed as:

$$\eta=4e\frac{\sinh kh}{\sinh 2kh+2kh}\sin kb\cos(k|x|-\sigma t) \quad \cdots\cdots(39)$$

The wave generating efficiency, or the ratio of the generated wave height to the stroke of the underwater piston, is then obtained from Eq. 31 as:

$$\frac{H}{2e}=\frac{4\sinh kh}{\sinh 2kh+2kh}\sin kb \quad \cdots\cdots(40)$$

It will be readily seen in Eq. 40 that this type of wave generator is very efficient in the shallow water but loses its efficieny as the water becomes deep. This characteristic is the opposite to the ordinary vertical-piston-type or flap-type generator which has a high efficiency in the deep water. Another characteristic is a peculiar nature that the wave height becomes null whenever the slot width $2b$

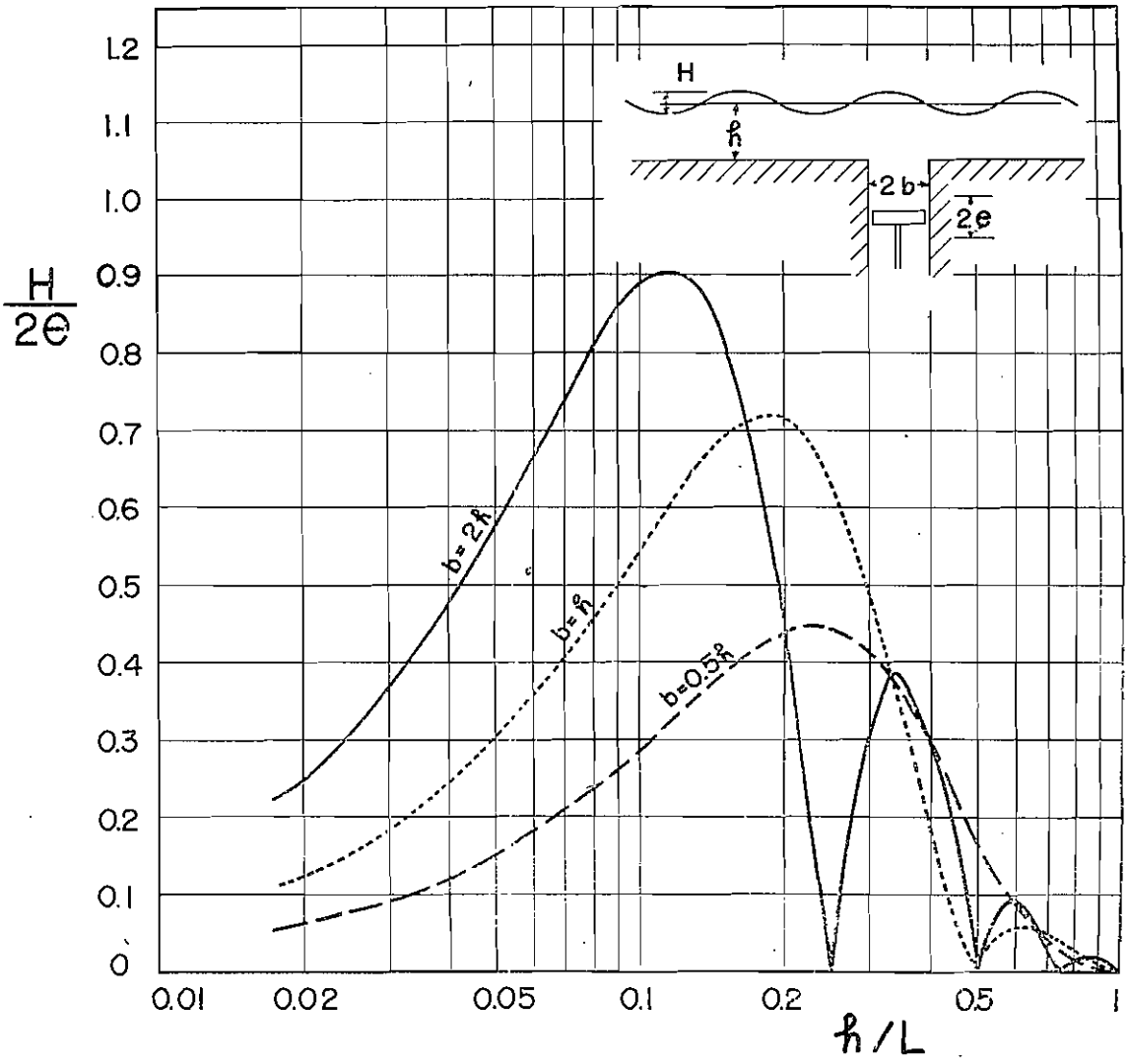

Fig. 3. Variation of $H/2e$ versus h/L for $b/h=0.5$, 1, and 2

coincides with a multiple of the wave length to be generated; this may be explained as due to the cancellation of positive wave generation with negative wave generation. Figure 3 shows the variation of the wave generating efficiency for the cases of $b=0.5h$, $1.0h$, and $2.0h$.

Bottom Pressure at the Wave Generating Area

The pressure variation at the bottom of the wave generating area ($|x|\leq b$ and $z=0$) can be calculated from the generalized Bernouille's equation as:

$$p=\rho\left[g(h-z)+\frac{\partial \Phi}{\partial t}\right]_{z=0} \quad \cdots\cdots(41)$$

The velocity potential for this case is the sum of ϕ_i with f_i given in Eq. 33 and of ϕ_s given by Eq. 35: i. e.,

$$\Phi_i=\phi_i+\phi_s=-f_i\cos\sigma t+f_s\sin\sigma t \quad \cdots\cdots(42)$$

The substitution of Eq. 42 into Eq. 41 yields the bottom pressure as:

$$p=\rho gh+\rho\sigma f_i(x, 0)\sin\sigma t+\rho\sigma f_s(x, 0)\cos\sigma t \quad \cdots\cdots(43)$$

The total pressure over the area of the oscillating flow, P, is then obtained by the integration of Eq. 43 from $x=-b$ to $x=b$. The result of the integration is written as:

$$P=B\int_{-b}^{b}pdx=2\rho gBbh+P_i\sin\sigma t+P_s\cos\sigma t \quad \cdots\cdots(44)$$

where: B=channel width

$$P_i=2\rho\sigma UBbh\left\{2\sum_{n=1}^{\infty}\frac{(1-e^{-2k_nh})}{k_nbk_nh(\sin 2k_nb+2k_nb)}-2\frac{\sin 2kb}{kb\,kb\,(\sinh 2kb+2kh)}-1+\frac{1}{kh\tanh kh}\right\} \quad \cdots\cdots(45)$$

$$P_s=8\rho\sigma UBbh\frac{\sin^2 kb}{kb\,kh\,(\sinh 2kh+2kh)} \quad \cdots\cdots(46)$$

The maximum total pressure is easily computed from Eq. 44 after the evaluation of P_i and P_s with Eqs. 45 and 46. Such a maximum pressure will give the maximum driving force of a moving channel bottom or of a piston placed very near to the channel bottom.

In actual designs of wave generators, however, a piston to generate the oscillating flow must be placed in a vertical cylinder or in a side tank connected to the cylinder. In these cases, the mass of water in the vertical cylinder and in the side tank is forced to oscillate in the same phase with the movement of a piston. The piston must be driven against the inertial force of the water mass in addition to the total pressure of Eq. 44. The driving force, therefore, is given by:

$$F=P_s\cos\sigma t+\left(P_i+\frac{\sigma U}{g}W\right)\sin\sigma t \quad\cdots\cdots(47)$$

where: W=weight of water mass moving in the same phase with piston. Some examples of numerical calculations by Eq. 47 are given in Table 2 in the next chapter.

Another interesting problem is the average rate of work done by the oscillating flow to the waves. The average rate of work, $\overline{\dot{W}}$, is calculated as:

$$\begin{aligned}\overline{\dot{W}}&=\frac{1}{T}\int_{-T/2}^{T/2}\int_{-b}^{b}p\left[-\frac{\partial\phi}{\partial z}\right]_{z=0}dx\,dt\\&=\frac{1}{T}\int_{-T/2}^{T/2}PU\cos\sigma t\,dt\\&=\frac{1}{T}\int_{-T/2}^{T/2}[2\rho gBbh+P_i\sin\sigma t+P_s\cos\sigma t]\,U\cos\sigma t\,dt\end{aligned}$$

Since the integrations of $\cos\sigma t$ and $\sin 2\sigma t$ over one wave period become zero, the above integration is rewritten as:

$$\overline{\dot{W}}=\frac{1}{T}\int_{-T/2}^{T/2}P_sU\cos^2\sigma t\,dt=4\sigma U^2B\frac{\sin^2kb}{k^2(\sinh 2kh+2kh)} \quad\cdots\cdots(48)$$

Using the result of Eq. 39 and the relation of $U=e\sigma$, the average rate of work of the oscillating flow is further rewritten as:

$$\overline{\dot{W}}=2\times\frac{1}{16}\rho g\frac{BH^2L}{T}\left(1+\frac{2kh}{\sinh 2kh}\right) \quad\cdots\cdots(49)$$

This is exactly the average rate of wave energy propagation into two directions.

III. SOME RESULTS AND DISCUSSIONS OF EXPERIMENTAL STUDY

Experimental Apparatus

In order to investigate the validity of the analysis developed, a small scale test has been carried out. A small wooden channel, 3.50 m long and 0.20 m wide, was constructed with a slot of 20 cm square at its center as shown in Fig. 4. The slot was connected to a side tank of 20 cm square at a depth of 36 cm below the channel bottom through a duct of 5 cm high and 20 cm wide. The side tank was provided with a piston of 20 cm square which was forced to oscillate sinusoidally in the vertical direction with a crank wheel and connecting rod mechanism. The oscillation of the piston thus produced a sinusoidally pulsating flow at the channel bottom. At the ends of the channel, wave absorbers of crushed stones with slopes of 1 to 4 were also provided.

The profiles of generated waves were recorded on an electro-magnetic oscillo-

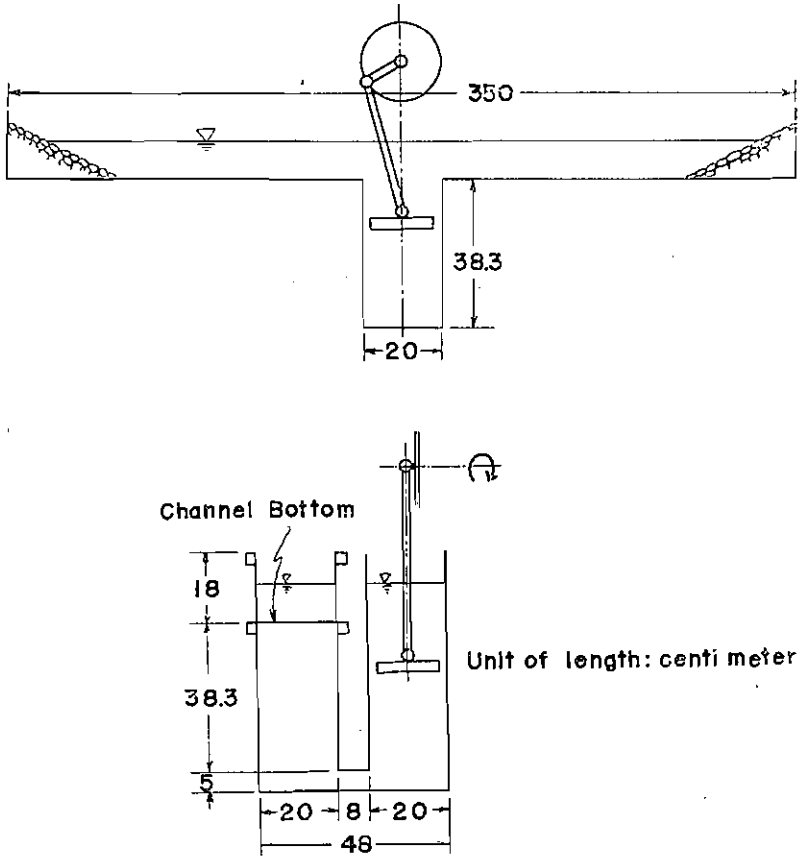

Fig. 4. Sketch of Test Channel

graph with resistance type wave gages. The forces required to drive the piston were also recorded with a load cell of strain-gage type which was inserted at the middle of the connecting rod. The wave periods were measured with an electronic time-counter which counted the time required for one rotation of the crank wheel up to four digits.

Profiles and Heights of Generated Waves

The first test was conducted at the water depth of 15 cm. The amplitude of the piston movement was set at $e=3$ cm and the period of the oscillation was varied from 2.02 to 0.612 seconds. Two wave gages were set in the channel, each 80 cm away form the center. Profiles of generated waves recorded with these gages were just the same as those generated by an ordinary piston-type or a flap-type wave maker.

The generated wave height varied from 1.24 to 2.95 cm The wave generating efficiency, or the ratio of the wave height to the stroke of the piston $2e$, varied from 0.206 to 0.492 accordingly. The variation of the efficiency is in good

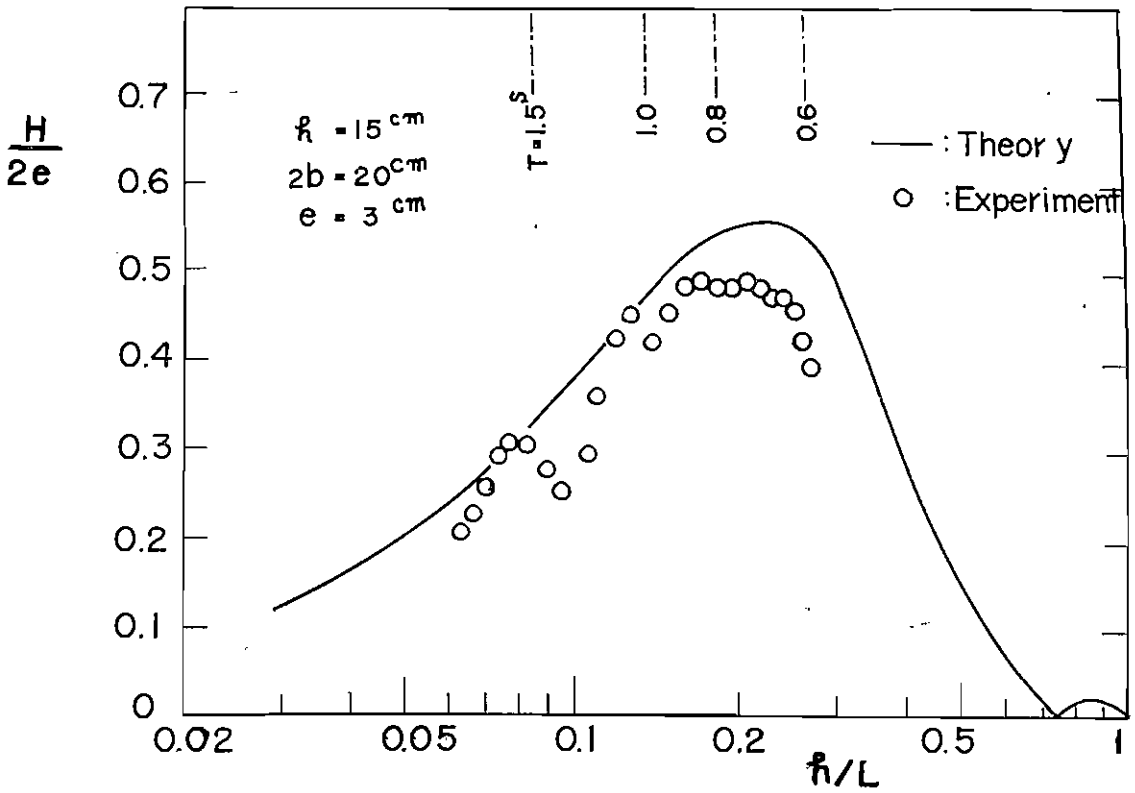

Fig. 5. Comparison of Experimental Values of $H/2e$ with Theoretical Ones

agreement with the analytical one of Eq. 40 as shown in Fig. 5, where the efficiency $H/2e$ is plotted against the relative depth h/L. The wave generating efficiency, both experimental and analytical ones, increases as the relative depth increases up to $h/L=0.2$, and then shows a decrease with the increase of h/L (or with the shortening of wave period). The experimental wave generating efficiency is about 80 per cent of the analytical one in the average. The smallness of the experimental efficieny may be explained as due to the energy dissipation caused by eddies around the edges of the slot and channel connection. The fluctuation of the experimental efficiency is considered as the result of partial reflections from the wave absorbers which were not efficient enough because of small space available; if the slope of crushed stone could have been made as gentle as 1 to 10, there would have been little fluctuation of the experimental efficiency.

Driving Force for the Piston

The measurement of driving forces for the piston was made for the amplitude of 3 cm for the piston movement at the water depth of 15 cm. The measurement was also made for the case of an empty tank. The driving force for the piston

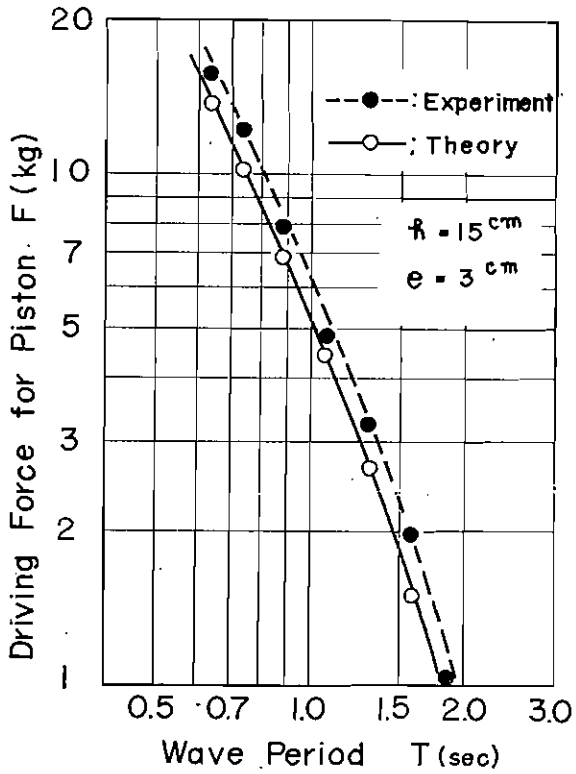

Fig. 6. Variation of Driving Force for Piston versus Wave Period

varied almost sinusoidally with respect to time. There was little indication of the second harmonic component appearance. The experimental data of the maximum driving forces (averages of peak values of tension and compression forces) are listed in Table 2 and shown in Fig. 6 as well as the results of the calculation by Eq. 47. Since the tests were made for two cases with and without water, the driving forces for the piston in the empty tank were subtracted from those in the tank filled with water to yield the net forces. These net driving forces were larger than the theoretical forces by the amount of 10 to 30 per cent as seen in Table 2 and Fig. 6. The weight of the water mass was 48.5 kg for this case with the increase of velocity at the duct being taken into consideration. The cause of the difference between theoretical and experimental forces is not clear; some portion of water in the channel near the slot may have been oscillated, thus increasing the effective weight of water mass.

As seen in Fig. 6, the driving force for the piston increases almost proportionally to the inverse square of wave period. This indicates the inertial force of the water mass being predominant. This fact is also illustrated in Table 2 in which the dynamic pressures of P_t and P_s become very small compared to the inertial force of $\sigma UW/g$ at short periods. For the purpose of a wave generator

design, the dynamic pressures of P_t and P_s may be neglected for the estimation of maximum driving force, provided the effective weight of the water mass being estimated reasonably.

TABLE 2. Experimental and Theoretical Driving Force for Piston.

T (sec)	F_w* (kg)	F_e** (kg)	$F_{exp}=F_w-F_e$ (kg)	P_s (kg)	P_t (kg)	$\frac{\sigma UW}{g}$ (kg)	F_{cal} (kg)
1.851	1.66	0.63	1.03	0.28	−0.92	1.71	0.83
1.584	2.55	0.57	1.98	0.32	−0.87	2.33	1.49
1.303	3.92	0.67	3.25	0.36	−0.81	3.45	2.66
1.069	5.58	0.78	4.80	0.39	−0.66	5.12	4.47
0.883	8.83	0.98	7.85	0.36	−0.59	7.52	6.93
0.740	13.2	1.12	12.1	0.30	−0.51	10.69	10.18
0.641	17.2	1.54	15.7	0.20	−0.59	14.28	13.69

Note: * F_w is the driving force in a tank with water
** F_e is the driving force in an empty tank

Reflection from Wave Generating Area

The last of the tests was concerned with the wave reflection from the wave generating area; unless a low reflection had not been proved, the present wave generator could not be said to be a practical one. Since a direct measurement of wave reflection from the generating area was difficult, an indirect method utilizing the multi-reflections between the wave generating area and a vertical wall was employed to estimate the magnitude of the wave reflection.

When a progressive wave is introduced in a region which has the complete wave reflection at one end and a partial wave reflection at the other end in a distance of l as shown in Fig. 7, the standing wave height at a vertical wall ($x=l$), H_s, is expressed as (see the Appendix for detail):

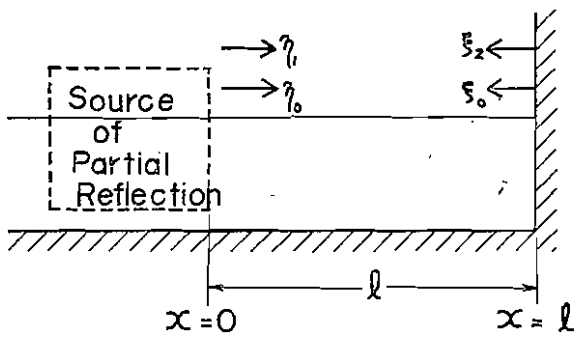

Fig. 7. Definition Sketch of Multi-Partial-Reflection System

$$H_s=\frac{2H_0}{[1+K_R^2-2K_R\cos 2kl]^{1/2}} \quad \cdots\cdots(50)$$

in which H_s is the height of the original progressive wave and K_R is the reflection coefficient. Therefore, the standing wave height H_s takes maximum values when $l=n\,L/2$ and mimnum values when $l=(2n+1)\,L/4$, in which n is an integer. The wave heights at these maxima and mimina are written as:

$$(H_s)_{\max}=\frac{2H_0}{1-K_R} \quad \cdots\cdots(51)$$

$$(H_s)_{\min}=\frac{2H_0}{1+K_R} \quad \cdots\cdots(52)$$

The reflection coefficient from the source of partial reflection is then obtained from Eqs. 51 and 52 assuming the constant height of the original wave as:

$$K_R=\frac{(H_s)_{\max}-(H_s)_{\min}}{(H_s)_{\max}+(H_s)_{\min}} \quad \cdots\cdots(53)$$

Although this analysis is an approximate one as seen in the Appendix, it nevertheless enables to estimate the magnitude of the reflection coefficient by measuring the variation of the standing wave height with respect to the wave period.

Based on the above analysis, the test was conducted with the wave absorber placed only at one end of the channel; the other end was kept vertical without a wave absorber. The water depth was set at 12 cm and the amplitude of the piston movement was 3 cm as before. The results of the measurement are shown in Fig. 8 where the wave generating efficiency $H/4e$ is plotted against the relative depth h/L. The denominator of $4e$ for the wave generating efficiency instead of $2e$ was so chosen because of the doubling of the wave height at the vertical wall. Although the upper envelope of the experimental data shows a good agreement with the theoretical efficiency, a periodic fluctuation of the experimental data with seven peaks is clearly seen in the figure. If the distance between the vertical wall of the channel and the outer end of the slot which is 185 cm for the present case is taken as the length of the multi-partial-reflection region l, the seven peaks of the experimental data fit very well with the analytical peak points of $l=nL/2$ for $n=2$ through $n=8$. Therefore, the wall at the outer end of the slot is considered to cause the partial reflection at the wave generating area.

By drawing two smooth lines connecting the maxima and minima of the experimental data and by measuring the maximum and minimum values of the wave generating efficiency for the same relative depth, the reflection coefficient of the wave generating area was calculated from Eq. 53 as 16 per cent in the average. This amount of the reflection coefficient indicates that 2.6 per cent of the wave energy was reflected at the wave generating area and the remaining

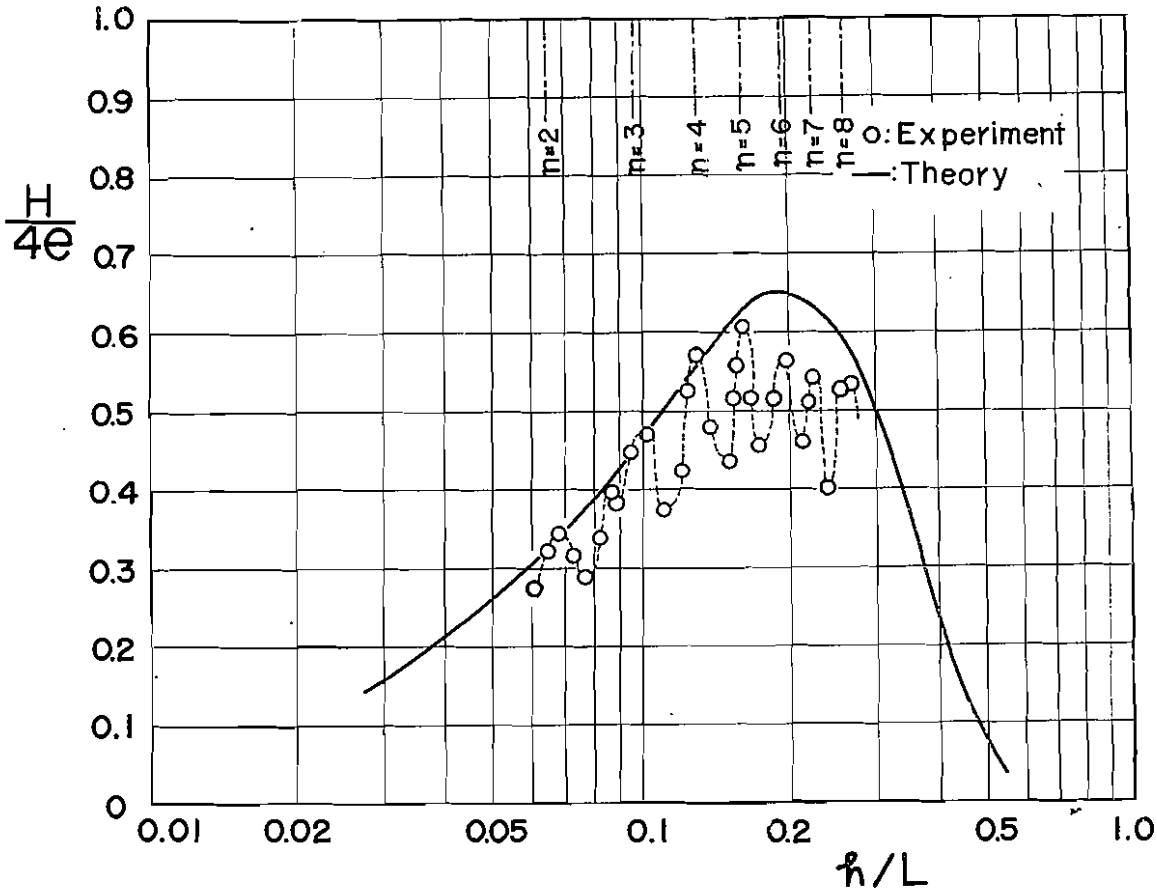

Fig. 8. Variation of Standing Wave Height versus Relative Depth

97.4 per cent of the wave energy traveled across it toward the other side of the channel, although some wave energy might have been dissipated by the turbulence around it. The transmission coefficient of the wave generating area is estimated as 98.7 per cent if the amount of energy dissipation is assumed to be negligible.

The high value of the transmission coefficient of the wave generating area was confirmed in the observation of the wave profiles at the other side of the channel which had the wave absorber. The wave heights at this part of the channel became less than 0.5 cm at the wave periods of 0.63, 0.82, and 1.34 seconds. These decreases of the wave heights are considered as the result of the superposi tion of two waves with their phase angles being different by 180 degrees. The condition for the opposite phase angles for the two waves, one generated and the other moving backward after the reflection at the vertical wall, is given by $l=(2n+1)\ L/2$ in which l is the distance of the vertical wall and the location of superposition. If l is taken as 185 cm, this condition gives the wave periods of 1.30 0.79, and 0.62 seconds for $n=1$ through $n=3$, showing a fairly good agreement with the observed periods.

IV. CONCLUSIONS

Summarizing the results of the preceding sections, the followings are the major conclusions of the present study:

1. The solution of velocity potential for water waves generated with a vertically oscillating flow at a channel bottom has been obtained, and expressions for wave profiles and bottom pressure at the wave generating area are derived from the velocity potential.
2. The experimental values of generated wave heights were about 80 per cent of the theoretical values for the range of the relative depth from 0.06 through 0.27.
3. The force required to drive an underwater piston which produces the oscillating flow is mainly of inertial force, being approximately proportional to the inverse square of the wave period. The experimental driving forces were some 20 per cent larger than the theoretical ones.
4. The reflection from the wave generating area was estimated as to be about 16 per cent; the reflection seems to be caused by the wall at the outer end of the vertical slot.
5. The method of water waves generation with a vertically oscillating flow at a channel bottom thus seems to be a very promising one to solve the problem of multi-reflection between a wave maker and model structures under study.

ACKNOWLEDGEMENT

The study presented herein was conducted at the Hydraulics Division of the Port and Harbour Technical Research Institute. The instrumentations employed were prepared by Mr. Suketo Haranaka, and the test channel was constructed by Mr. Takao Kitatani. The authors hereby sincerely appreciates the assistances of Messrs. Haranaka and Kitatani.

The authors also wish to express their appreciations to Mr. Yoshiyuki Ito, Chief of the Breakwater Laboratory, for his critical review of the manuscript and valuable suggestions to it.

REFERENCES

Goda, Yoshimi 1962: "A Method to Measure the Coefficient of Transmission of a Filter in a Closed Basin," *Uupublished Paper, Massachusetts Institute of Technology, Hydrodynamics Laboratory.*

Ippen, A. T., Raichlen, F., and Sullivan, R. K. Jr. 1962: "Wave Induced Oscilla-

tions in Harbors: Effect of Energy Dissipators in Coupled Basin System," *Massachusetts Institute of Technology, Hydrodynamics Laboratory, Report No. 52,* 49 pp.

Iwagaki, Y., Tsuchiya, Y., and Inoue M. 1962: "Study on the Wave Overtoppings for Sea Walls in a Wind-Wave Channel (1)," *Proc. 9th Conf. Coastal Eng. in Japan, JSCE,* pp. 153–158.

Stoker, J. J. 1957: "Water Waves," *Interscience Publishers,* New York, 567 pp.

APPENDIX

Water Surface Profiles in a Multi-Partial-Reflection System

An analysis of the water surface profiles in a multi-partial-reflection system has been developed by the author (1962) and presented in the report by Ippen, Raichlen, and Sullivan (1962) for the purpose to estimate the transmission coefficient of a wave filter in a closed basin. The analysis can easily be modified to the system shown in Fig. 7 so as to describe the variation of the wave heights in the system, as shown in the following.

In the analysis the following assumptions are imposed:

i) Small amplitude wave theory applies.

ii) Waves are reflected completely at $x=l$ and reflected partially at $x=0$ with the reflection coefficient of $\boldsymbol{K}_R$.

iii) The n-th reflected wave can be superposed on the original progressive wave.

The original progressive wave introduced in the system is expressed as:

$$\eta_1=A_0\cos(\sigma t-kx) \quad \cdots\cdots(A.1)$$

This original progressive wave is reflected completely at the vertical wall of $x=l$, following the first retrogressive wave:

$$\zeta_1=A_0\cos(\sigma t+kx-2kl) \quad \cdots\cdots(A.2)$$

When this retrogressive wave returns to the origin, a part of the wave is reflected and the following second progressive wave is formed:

$$\eta_2=\boldsymbol{K}_R A_0\cos(\sigma t-kx-2kl) \quad \cdots\cdots(A.3)$$

As before this progressive wave is reflected at $x=l$. The resultant second retrogressive wave is described by:

$$\zeta_2=\boldsymbol{K}_R A_0\cos(\sigma t+kx-4kl) \quad \cdots\cdots(A.4)$$

In a similar manner two families of progressive waves (η_n) and retrogressive waves (ζ_n) may be defined, their amplitudes decreasing progressively with increasing n due to the multi-partial-reflections at the origin.

The wave system which ultimately exists between the source of partial reflec-

tion and vertical wall may then be expressed as the sum of all the progressive and reflected waves.

$$\eta=\eta_1+\zeta_1+\eta_2+\zeta_2+\cdots+\eta_n+\zeta_n+\cdots \quad \cdots\cdots(A.5)$$

Since these waves may also be expressed as the real parts of complex numbers, i. e.:

$$\eta_n=\boldsymbol{K}_R^{n-1}A_0\cos[\sigma t-kx-2(n-1)kl]$$
$$=\text{Real}\{\boldsymbol{K}_R^{n-1}A_0\exp[i(\sigma t-kx)]\times\exp[-2i(n-1)kl]\}$$

the resultant wave of Eq. A. 5 may be expressed as:

$$\eta=\text{Real}\Big[A_0\{\exp[i(\sigma t-kx)]+\exp[i(\sigma t+kx-2kl)]\}$$
$$\times\{1+\boldsymbol{K}_R\exp[-2ikl]+\boldsymbol{K}_R^2\exp[-4ikl]+\cdots\}\Big] \quad \cdots\cdots(A.6)$$

For an absolute value of the reflection coefficient less than one, this series converges to:

$$\eta=\text{Real}\Big[\frac{A_0}{1-\boldsymbol{K}_R\exp[-2ikl]}\{\exp[i(\sigma t-kx)]+\exp[i(\sigma t+kx-2kl)]\}\Big]$$
$$\cdots\cdots(A.7)$$

Taking the real part of Eq. A. 7, we obtain the expression for the wave profile in the multi-partial-reflection system as:

$$\eta=\frac{A_0}{1+\boldsymbol{K}_R^2-2\boldsymbol{K}_R\cos 2kl}\{\cos(\sigma t-kx)+\cos(\sigma t+kx-2kl)$$
$$-\boldsymbol{K}_R\cos(\sigma t-kx+2kl)-\boldsymbol{K}_R\cos(\sigma t+kx)\} \quad \cdots(A.8)$$

This equation expresses the displacement of the water surface from mean water level as a function of time for any location between the source of partial reflection and the vertical wall of the channel. The wave profile at the vertical wall is obtained simply by letting $x=l$ in Eq. A. 8, i. e.:

$$\eta|_{x=l}=\frac{H_0}{1+\boldsymbol{K}_R^2-2\boldsymbol{K}_R\cos 2kl}\{\cos(\sigma t-kl)-\boldsymbol{K}_R\cos(\sigma t+kl)\}\cdots\cdots(A.9)$$

in which $H_0=2A_0$ is the height of the original progressive wave. The standing wave height at the vertical wall of the channel is then derived from the above equation after some trigonometric manipulations. The final form of the standing wave height becomes:

$$H_s=\frac{2H_0}{[1+\boldsymbol{K}_R^2-2\boldsymbol{K}_R\cos 2kl]^{1/2}} \quad \cdots\cdots(A.10)$$

which is Eq. 50 in the text.